

HOLLOW BEAM FORMATION IN THE INTENSE MULTI-COMPONENT HEAVY ION BEAM CAUSED BY BEAM SELF-FIELD

N. Kazarinov

Joint Institute for Nuclear Research, Dubna

The simulation of the hollow beam formation in the intense multi-component ion beam from ECR source is fulfilled. The influence of the helium and hydrogen beam current on the argon and calcium ions dynamics has been studied.

Проведено моделирование формирования трубчатого пучка в многокомпонентном ионном пучке, получаемом в ЭЦР-источнике. Изучается влияние пучков ионов гелия и водорода на динамику пучков ионов аргона и кальция.

PACS: 29.27.Bd

INTRODUCTION

The initial part of the injection beam line of NSCL MSU cyclotron K500 consists of the focusing solenoids and analyzing double focusing bending magnet. The focusing length of the solenoid for the lighter ions (that is the ion with the smaller mass-to-charge ratio) is less than for one injected into cyclotron. For this reason in the region between the solenoid and the analyzing magnet the lighter ion beams have significantly smaller transverse dimensions compared to injected beam ones. In the region out of the lighter ion beam boundary, the defocusing field decreases as inverse distance of the ions from the axis of the beam. For big magnitude of the lighter ion beam space charge, this leads to formation of the hollow beam of injected ions just after analyzing magnet and increases the emittance of injected ion beam.

This effect has been observed in the computer simulation [1] and experimentally in the NSCL injection beam line during injection of $^{48}\text{Ca}^{6+}$ ions [2].

In this work the simulation of the argon and calcium beams transportation in the initial part of the NSCL injection beam line has been performed. The influence of the helium and hydrogen beam current on the argon and calcium ions dynamics has been studied as well.

The replacement of the focusing solenoid by triplet of the electrostatic lenses could eliminate the effect of hollow beam formation. The parameters of such a triplet (apertures and plate voltages) for achieving the high transportation efficiency (100%) have been found.

The simulation has been performed with the help of Multi-Component Ion Beam code (MCIB-04) [3] created at the Joint Institute for Nuclear Research, Dubna, Russia.

This article was written in September–October 2004 during author's work at NSCL MSU. After this the main results of this work have been confirmed by a lot of experimental data [5–7].

1. SIMULATION OF THE HOLLOW BEAM FORMATION IN THE ARGON BEAM

The scheme of the initial part of the NSCL injection beam line is shown in Fig. 1. The longitudinal magnetic field in the beam line is shown in Fig. 2.

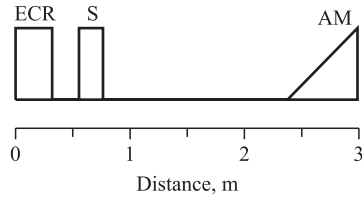


Fig. 1. Scheme of the beam line: ECR — longitudinal magnetic field of the ECR-ion source; S — focusing solenoid; AM — 90° analyzing magnet

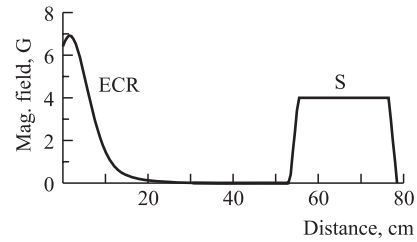


Fig. 2. Longitudinal magnetic field in the beam line

Table 1. Argon beam parameters

Ion mass	40
Ion charge	2–12
Central (injected) charge	7
ECR extraction voltage, kV	24.43
Kinetic energy (central charge), keV/m.u.	4.3
Beam diameter, mm	8
Beam emittance (central charge), π mm-mrad	100
Total current, mA	2.31
Central charge current, μA	275

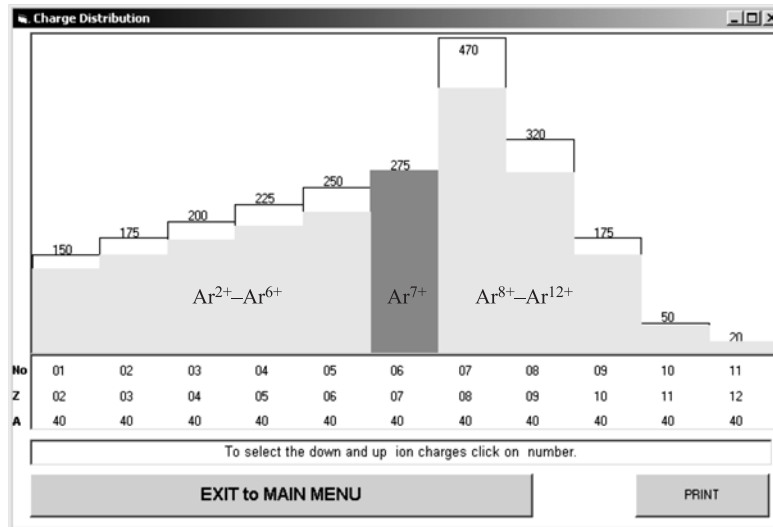


Fig. 3. Argon beam spectrum. Total beam current — 2.31 mA. No — ordinal number of the ion species; Z, A — charge and mass of the ion. Upper numbers are the currents of the different charge states of the beam in μA

The simulation has been performed for argon beam. The parameters of the beam are contained in Table 1. The argon beam spectrum is shown in Fig. 3.

The computed trajectories of the particles of the argon beam are shown in Fig. 4. The magnetic field induction of the solenoid is equal to 4 kG. The lighter ions have smaller envelopes just after the solenoid. The transportation efficiency of the $^{40}\text{Ar}^{7+}$ ions in this case is equal to 100%.

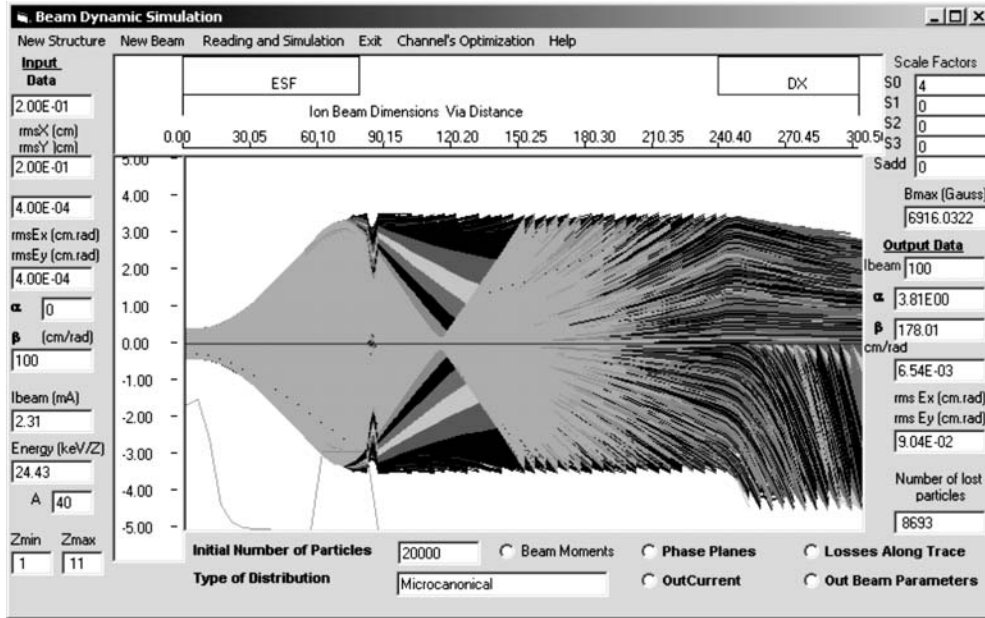


Fig. 4. Argon ion trajectories

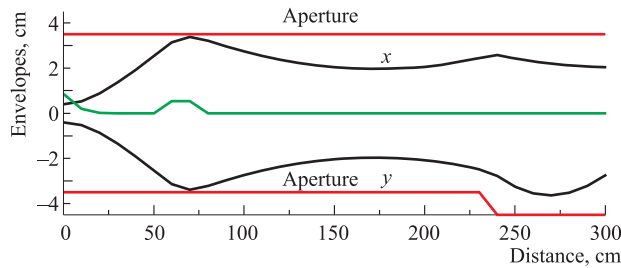
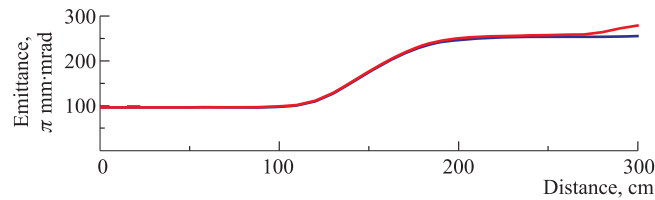
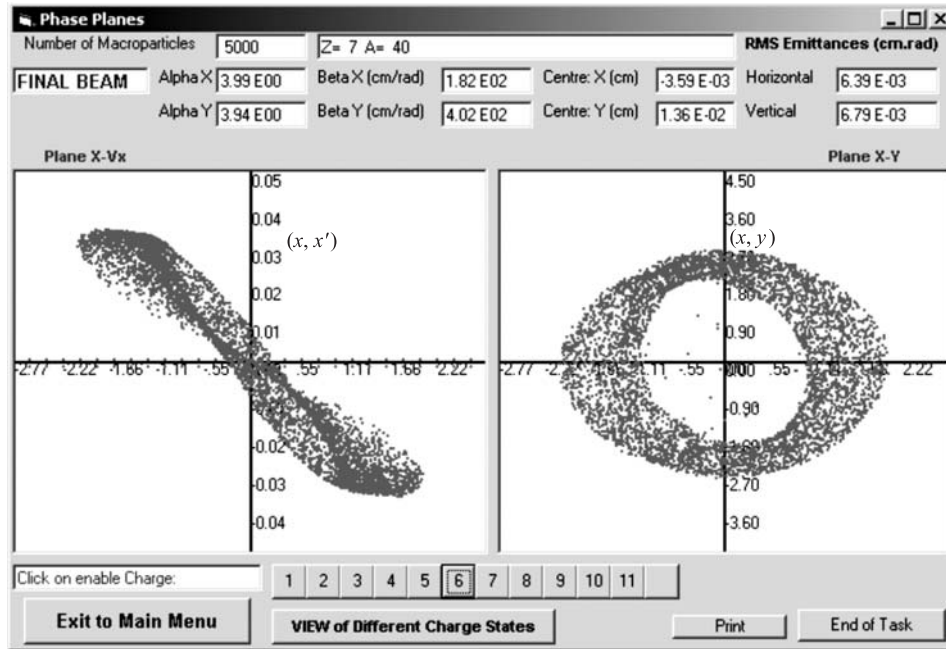


Fig. 5. Horizontal (x) and vertical (y) envelopes of the $^{40}\text{Ar}^{7+}$ ion beam

The $^{40}\text{Ar}^{7+}$ ion beam envelopes are shown in Fig. 5. The dependence of the beam emittance on the distance along the beam line is given in Fig. 6.

As may be seen, the increasing of the emittance begins just after the solenoid and achieves the maximum value $250 \pi \text{ mm} \cdot \text{mrad}$, which is in 2.5 times greater than the initial one. The $^{40}\text{Ar}^{7+}$ ions distributions just after the analyzing magnet at the (x, y) plane (right) and (x, x') plane (left) are shown in Fig. 7.

Fig. 6. Emittance of the $^{40}\text{Ar}^{7+}$ ion beamFig. 7. The $^{40}\text{Ar}^{7+}$ ions distributions just after the analyzing magnet

As may be seen from Fig. 7, the $^{40}\text{Ar}^{7+}$ beam has a hole and strong nonlinear distortions of the beam emittances. In this case the appearance of the hole is connected with the presence of the charges greater than the central one in the argon beam spectrum. For checking this assumption, the argon beam with charges smaller than the central one have been considered. The argon beam spectrum for this case is shown in Fig. 8. The particles distributions just after the analyzing magnet are given in Fig. 9.

In the considered case the lower charge state beams have greater transversal dimensions than the central ones. For this reason there are no both hole and nonlinear distortion of the emittance in the $^{40}\text{Ar}^{7+}$ beam.

The appearance of the hole in the $^{40}\text{Ar}^{7+}$ beam depends on the type of the lighter ions. In the case of the transportation of both the $^{40}\text{Ar}^{2+-7+}$ ions and the proton beams, the hole in the $^{40}\text{Ar}^{7+}$ beam disappears. The argon and proton beam spectrum is shown in Fig. 10. The Ar^{7+} distributions are given in Fig. 11.

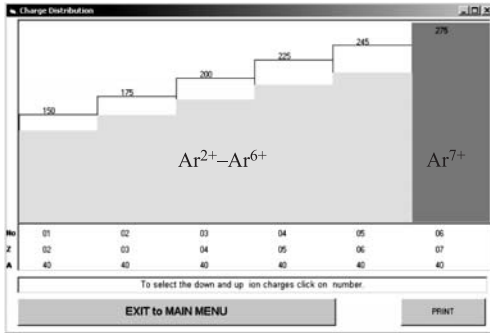


Fig. 8. Argon beam spectrum with lower charge states. The designations are the same as in Fig.3

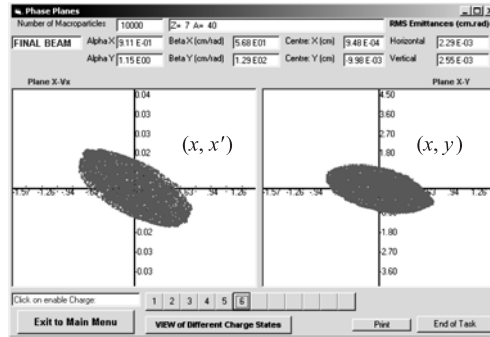


Fig. 9. The $^{40}\text{Ar}^{7+}$ ions distributions just after the analyzing magnet

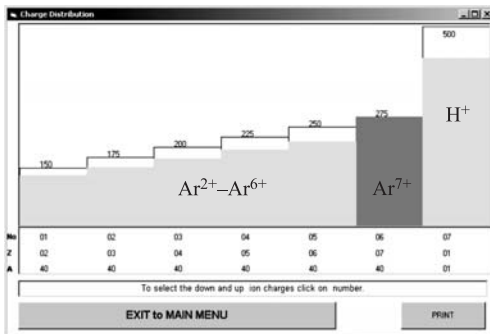


Fig. 10. Argon and proton beam spectrum. The designations are the same as in Fig.3

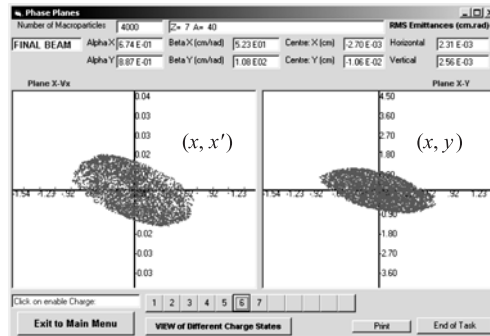


Fig. 11. The $^{40}\text{Ar}^{7+}$ ions distributions just after the analyzing magnet

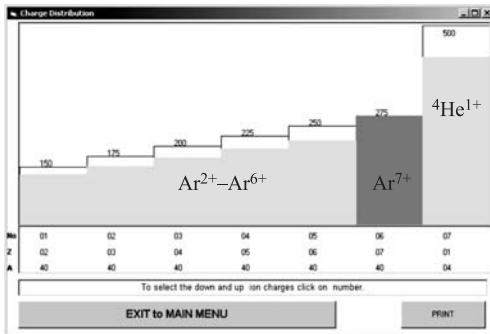


Fig. 12. Argon and $^4\text{He}^{1+}$ beam spectrum. The designations are the same as in Fig.3

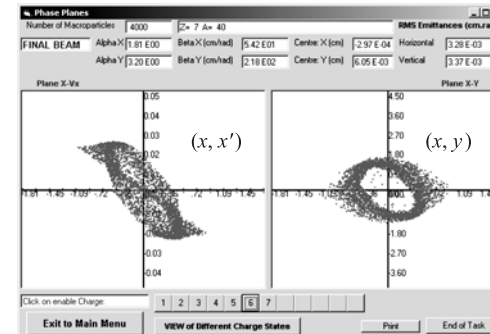


Fig. 13. The $^{40}\text{Ar}^{7+}$ ions distributions just after the analyzing magnet

The hole disappears because the protons go away from the argon beam very fast and therefore its influence on the argon ions is very small. If instead of proton beam the ion beam with mass-to-charge ratio equal to 2 (that is $^2\text{H}^{1+}$ or $^4\text{He}^{2+}$ ions) is considered, the hole in

the $^{40}\text{Ar}^{7+}$ disappears almost completely. For ion beam with mass-to-charge ratio equal to 4 (that is $^4\text{He}^{1+}$ ions), the hole in the $^{40}\text{Ar}^{7+}$ appears again. The spectrum of the argon and $^4\text{He}^{1+}$ beams is shown in Fig. 12. The particles distributions just after the bending magnet are given in Fig. 13.

2. SIMULATION OF THE HOLLOW BEAM FORMATION IN THE CALCIUM BEAM

The beam of ^{40}Ca and ^{48}Ca ions is obtained in ECR-ion source with helium as plasma-supporting gas. The parameters of the ^{40}Ca and helium beam current are contained in Table 2.

The spectrum of the ^{40}Ca and helium ions beam is shown in Fig. 14. The computed trajectories of the particles of the ^{40}Ca and helium beam are shown in Fig. 15. The magnetic

Table 2. ^{40}Ca and helium beam parameters

Ion mass	40
Ion charge	2–12
Central (injected) charge	8
ECR extraction voltage, kV	24.43
Kinetic energy (central charge), keV/m.u.	4.3
Beam diameter, mm	8
Beam emittance (central charge), π mm · mrad	100
Total current, mA	2.028
Central charge current, μA	156
$^4\text{He}^{1+}$ beam current, μA	1000
$^4\text{He}^{2+}$ beam current, μA	200

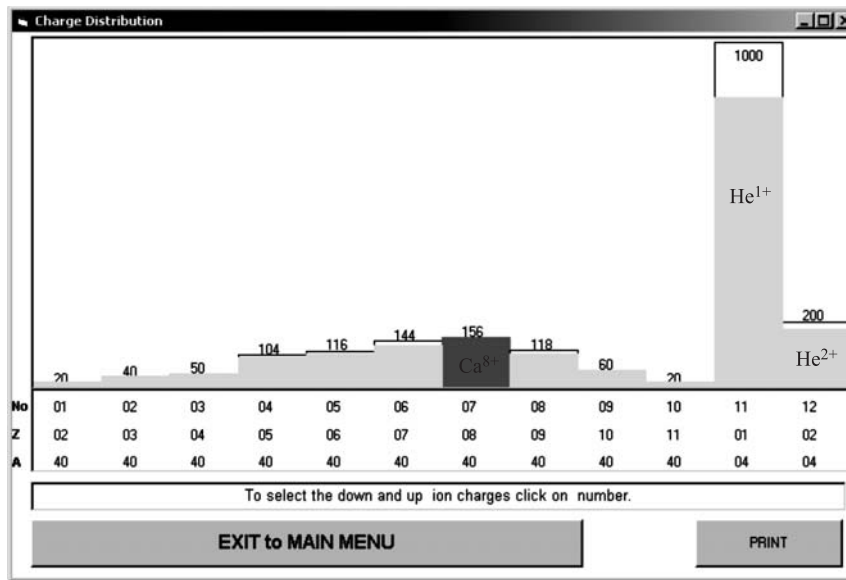


Fig. 14. The spectrum of the ^{40}Ca and helium ions beam. The designations are the same as in Fig. 3

field induction of the solenoid is equal to 4.1 kG. The transportation efficiency of the $^{40}\text{Ca}^{8+}$ ions in this case is equal to 100%.

The $^{40}\text{Ar}^{7+}$ ion beam envelopes are shown in Fig.16. The dependence of the beam emittance on the distance along the beam line is given in Fig.17. As may be seen, the emittance achieves the maximum value $180 \pi \text{ mm} \cdot \text{mrad}$, which is 1.8 times greater than the initial one. The $^{40}\text{Ca}^{8+}$ ions distributions just after the analyzing magnet are shown in Fig. 18.

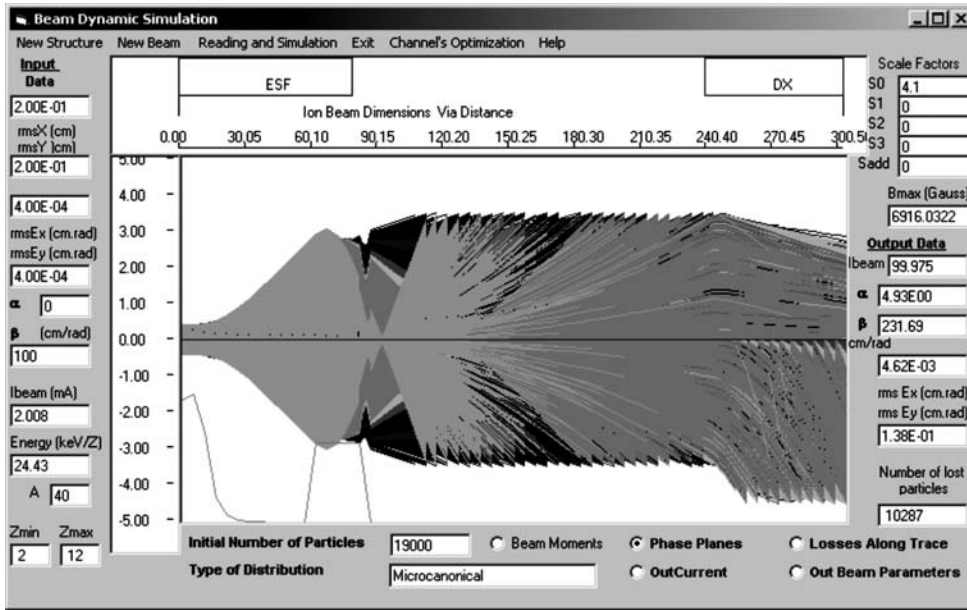


Fig. 15. ^{40}Ca and helium ion trajectories

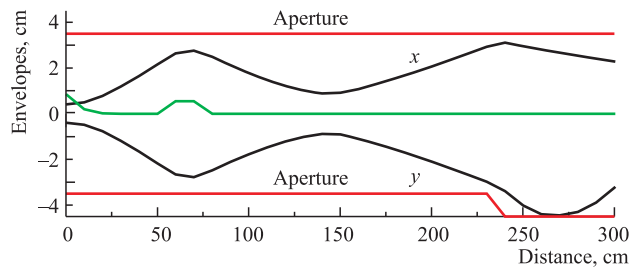


Fig. 16. Horizontal (x) and vertical (y) envelopes of the $^{40}\text{Ca}^{8+}$ ion beam

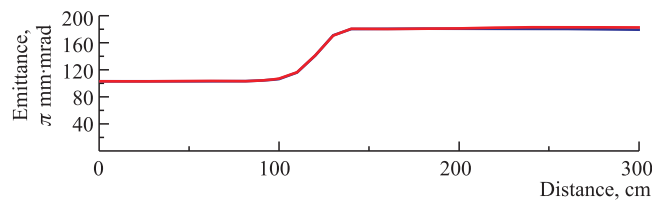


Fig. 17. $^{40}\text{Ca}^{8+}$ beam emittance

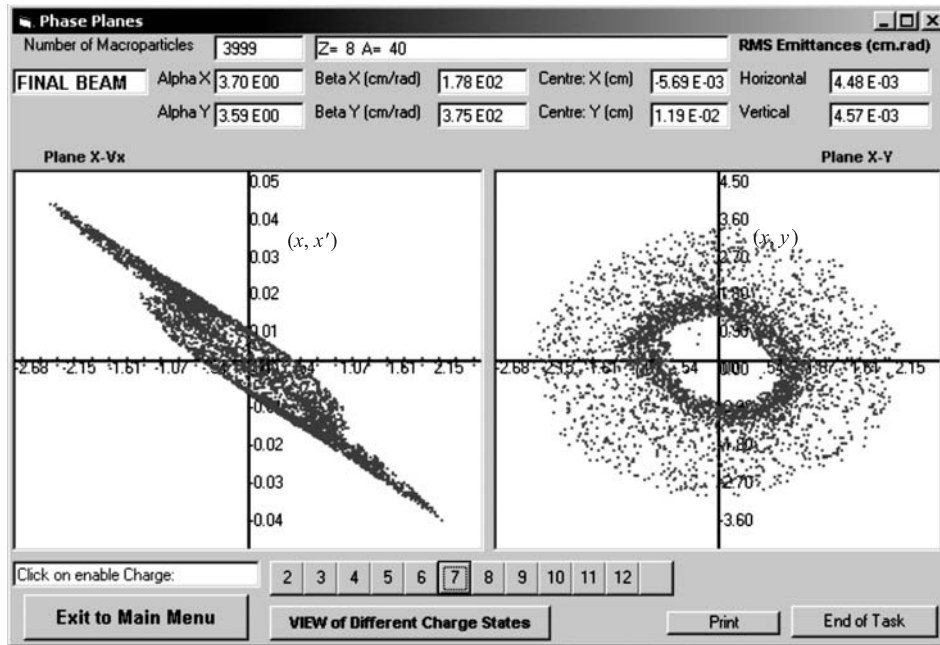


Fig. 18. The $^{40}\text{Ca}^{8+}$ ions distributions just after the analyzing magnet. Calcium beam transportation with helium beam

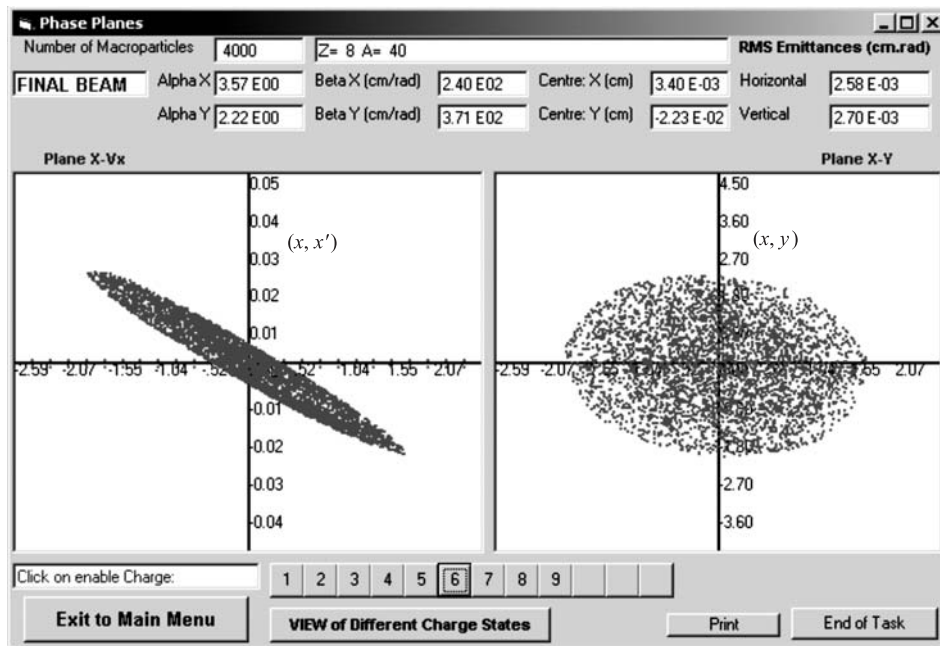


Fig. 19. The $^{40}\text{Ca}^{8+}$ ions distributions just after the analyzing magnet. Calcium beam transportation without helium beam

As may be seen from Fig. 18, the $^{40}\text{Ca}^{8+}$ beam has a hole and strong nonlinear distortion of the emittance. In contradiction to the transportation of the argon ions, the hollow beam formation is caused by helium ions only. The simulation of the Ca beam transportation without helium ions shows that there is no hole in the $^{40}\text{Ca}^{8+}$ in this case. The corresponding $^{40}\text{Ca}^{8+}$ ions distributions are given in Fig. 19.

3. FOCUSING BY TRIPLET OF ELECTROSTATIC LENSES

The replacement of the focusing solenoids by the triplet of the electrostatic lenses eliminates the hollow beam formation because of the focus length of the electrostatic lens independent on charge-to-mass ratio of the ions obtained in the ECR-ion source. The scheme of the initial part of the NSCL injection beam line with the focusing by the electrostatic lens triplet is shown in Fig. 20. The entrance of the first lens coincides with the beginning of the focusing solenoid in the existing beam line (Fig. 1).

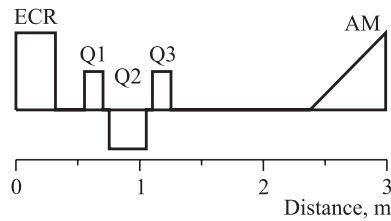


Fig. 20. Scheme of the triplet focusing. Q1–3 — electrostatic lenses

The simulation was performed in two stages. At the first stage the gradients of the lenses have been fitted by using the code based on the moments method. This code is the part of the program library MCIB-04 [3]. The fitted gradients give the possibility to achieve 100%-transmission efficiency through the analyzing magnet. At the second stage the simulation was performed with the help of the macro particles code. The argon ion trajectories calculated at second stage are shown in Fig. 21. The envelopes of

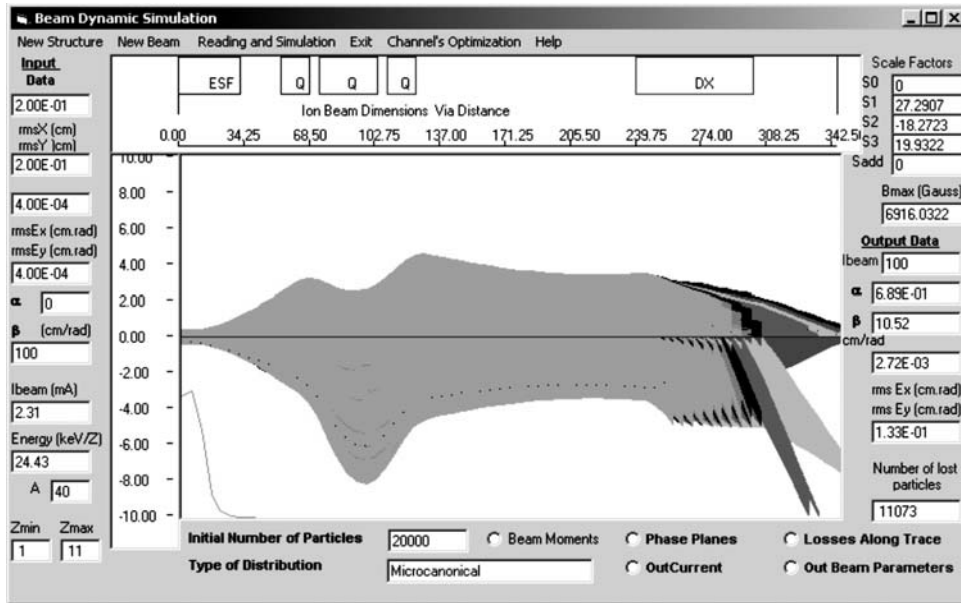


Fig. 21. Argon ion trajectories

the $^{40}\text{Ar}^{7+}$ beam obtained by two simulation methods are given in Fig. 22. As may be seen from Fig. 22, both methods give the same envelopes of the beam.

The magnitude of the vertical beam envelope inside the middle lens of the triplet is equal to 80 mm. Therefore, inner diameter of lens poles must be not less than 200 mm. For such

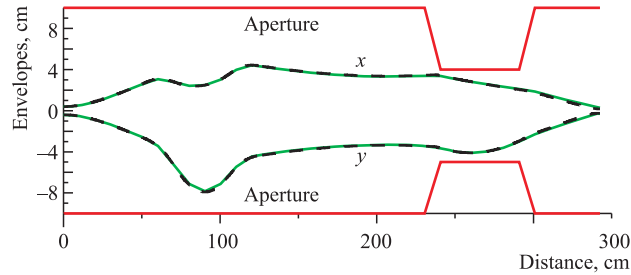


Fig. 22. Horizontal (x) and vertical (y) $^{40}\text{Ar}^{7+}$ beam envelopes. Dashed line — moments method; solid line — macro particles

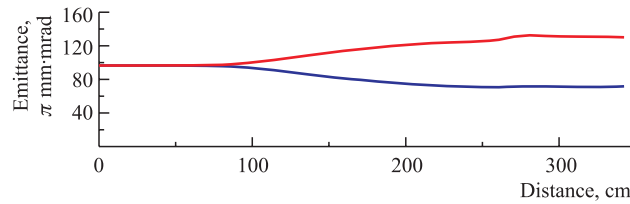


Fig. 23. Horizontal (x) and vertical (y) emittances of the $^{40}\text{Ar}^{7+}$ beam

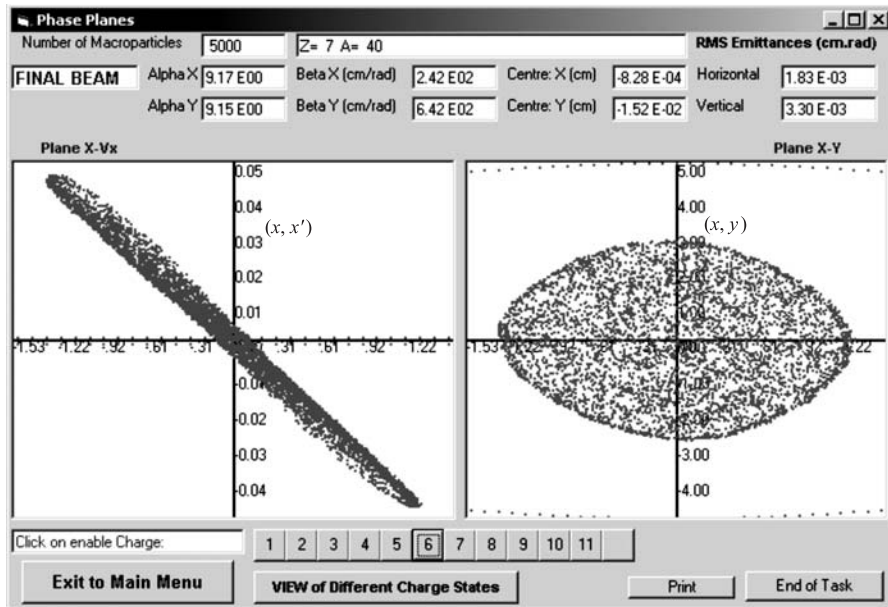


Fig. 24. The $^{40}\text{Ar}^{7+}$ ions distributions just after the analyzing magnet. Electrostatic triplet focusing

an aperture the pole voltages of the lenses are 6.7, -4.5, 4.9 kV correspondingly. The pole face rotation angle of analyzing magnet has been reduced down to 25.2° instead of actual value 30.7° to achieve the beam crossover at the final point of the simulation.

The dependences of the beam emittances on distance along the beam line are shown in Fig. 23. The difference between horizontal and vertical emittances arise from the coupling caused by self-field of the non-axial symmetric rotating beam.

As may be seen from Fig. 21, there are no intermediate foci of the lighter ions. For this reason the $^{40}\text{Ar}^{7+}$ beam has no hole. This is illustrated by particles distributions shown in Fig. 24.

Decreasing of the aperture of the electrostatic lenses leads to the particle losses during transportation. Thus, for example, for actual lens aperture $\varnothing 100$ mm and with the mask at the entrance of the first lens with hole $\varnothing 50$ mm, the transmission efficiency decreases down to 60%.

REFERENCES

1. Kazarinov N. Yu. Non-Linear Distortion of Multi-Component Heavy Ion Beam Emittance Caused by Space Charge Fields // Proc. of the 14th Intern. Conf. on Ion Sources, Dubna, 2003; Rev. Sci. Instr. 2004. V. 75. P. 1665.
2. Stetson J. W. et al. A Comparison of Electrostatic and Magnetic Focusing of Mixed Species Heavy Ion Beams at NSCL/MSU // Proc. of 17th Intern. Conf. on Cycl. «Cyclotrons'04», Tokyo, Japan, Oct. 18–22, 2004.
3. Kazarinov N., Aleksandrov V., Shevtsov V. Multi-Component Ion Beam Code — MCIB-04 // Proc. of XIX Rus. Particle Acc. Conf. «RuPAC2004», Dubna, Oct. 4–9, 2004. P. 201.
4. Leitner M. et al. // Proc. of the 15th Intern. Workshop on ECR Ion Source, Jyvaskyla, Finland, June 12–14, 2002. P. 32–34.
5. Stetson J. W. et al. Experimental Comparison of Electrostatic and Magnetic Solenoid Focusing of Low Energy Heavy Ion Beam at NSCL/MSU // Proc. of the 2005 Part. Acc. Conf. «PAC05», Knoxville, Tennessee, USA, May 16–20, 2005.
6. Koivisto H. et al. Program to Improve the Ion Beam Formation and Transmission at JYFL // Proc. of 18th Intern. Conf. on Cycl., Giardini Naxos, Italy, Sept. 30–Oct. 5, 2007.
7. Koivisto H. et al. Development of Metal Ion Beams and Beam Transmission at JYFL // Proc. of 11th Intern. Conf. on Heavy Ion Acc. Techn. «HIAT09», Venezia, Italy, June 8–12, 2009.

Received on July 23, 2009.